JCI insight

RESEARCH ARTICLE

TNF receptor–activated factor 2 mediates cardiac protection through noncanonical NF-κB signaling

Sarah Evans,[1] Huei-Ping Tzeng,[1] Deborah J. Veis,[2] Scot Matkovich,[1] Carla Weinheimer,[1] Attila Kovacs,[1] Philip M. Barger,[1] and Douglas L. Mann[1]

[1]Center for Cardiovascular Research, Cardiovascular Division and [2]Division of Bone and Mineral Metabolism, Department of Medicine, Washington University School of Medicine, St. Louis, Missouri, USA.

To elucidate the mechanisms responsible for cytoprotective effects of TNF receptor–activated factor 2 (TRAF2) in the heart, we employed genetic gain- and loss-of-function studies ex vivo and in vivo in mice with cardiac-restricted overexpression of TRAF2 (*Myh6*-TRAF2$_{LC}$). Crossing *Myh6*-TRAF2$_{LC}$ mice with mice lacking canonical signaling (*Myh6*-TRAF2$_{LC}$/*Myh6*-IκBαΔN) abrogated the cytoprotective effects of TRAF2 ex vivo. In contrast, inhibiting the JAK/STAT pathway did not abrogate the cytoprotective effects of TRAF2. Transcriptional profiling of WT, *Myh6*-TRAF2$_{LC}$, and *Myh6*-TRAF2$_{LC}$/*Myh6*-IκBαΔN mouse hearts suggested that the noncanonical NF-κB signaling pathway was upregulated in the *Myh6*-TRAF2$_{LC}$ mouse hearts. Western blotting and ELISA for the NF-κB family proteins p50, p65, p52, and RelB on nuclear and cytoplasmic extracts from naive 12-week-old WT, *Myh6*-TRAF2$_{LC}$, and *Myh6*-TRAF2$_{LC}$/*Myh6*-IκBαΔN mouse hearts showed increased expression levels and increased DNA binding of p52 and RelB, whereas there was no increase in expression or DNA binding of the p50 and p65 subunits. Crossing *Myh6*-TRAF2$_{LC}$ mice with RelB$^{-/+}$ mice (*Myh6*-TRAF2$_{LC}$/RelB$^{-/+}$) attenuated the cytoprotective effects of TRAF2 ex vivo and in vivo. Viewed together, these results suggest that crosstalk between the canonical and noncanonical NF-κB signaling pathways is required for mediating the cytoprotective effects of TRAF2.

Introduction

In response to myocardial injury, the adult heart is capable of synthesizing an ensemble of proteins that enable and facilitate cardiac repair and left ventricular (LV) remodeling. We and others have shown that cytokines released by cardiocytes and professional immune cells residing within the myocardium confer cytoprotective responses following myocardial injury (1). TNF, which is among the most studied cytokines released by the heart following tissue injury, provokes cell survival responses in isolated cardiac myocytes (2, 3) and confers protective responses following coronary artery ligation and/or ischemia reperfusion (I/R) injury (4–7). Thus far, 3 different mechanisms have been proposed to explain the cytoprotective effects of TNF, including activation of the neutral sphingomyelinase pathway through generation of ceramide and/or sphingosine 1-phosphate (6), activation of the JAK/STAT pathway by the survivor activating factor enhancement (SAFE) pathway (8), and most recently TNF-induced activation of TNF receptor–activated factor 2 (TRAF2) (9–11).

TRAF2 is a canonical member of the TRAF family (TRAF1–7) of proteins that exhibit shared modular domains characteristic of adapter proteins. TRAFs are critical for mediating signal transduction pathways initiated by members of the TNF receptor family (TNFR), the TLR family, the IL-1 receptor family, and the RIG-I–like receptor family. All TRAF family members, with the exception of TRAF1, contain a RING finger domain localized at their N-terminus. The RING finger domain is common to many E3 ubiquitin ligases, which are crucial for the activation of downstream signaling pathways. TRAF proteins mediate signaling through the canonical NF-κB1 and noncanonical NF-κB2 pathways, mitogen-activated protein kinases, and IFN-regulatory factors. Functionally, TRAFs control a plethora of diverse cellular processes, including cell survival, tissue homeostasis, cell proliferation, differentiation, cytokine production, autophagy, and mitophagy (11, 12). We have shown that the cytoprotective effects of TRAF2 are mediated,

Conflict of interest: The authors have declared that no conflict of interest exists.

Submitted: October 23, 2017
Accepted: January 5, 2018
Published: February 8, 2018

Reference information:
JCI Insight. 2018;3(3):e98278. https://doi.org/10.1172/jci.insight.98278.

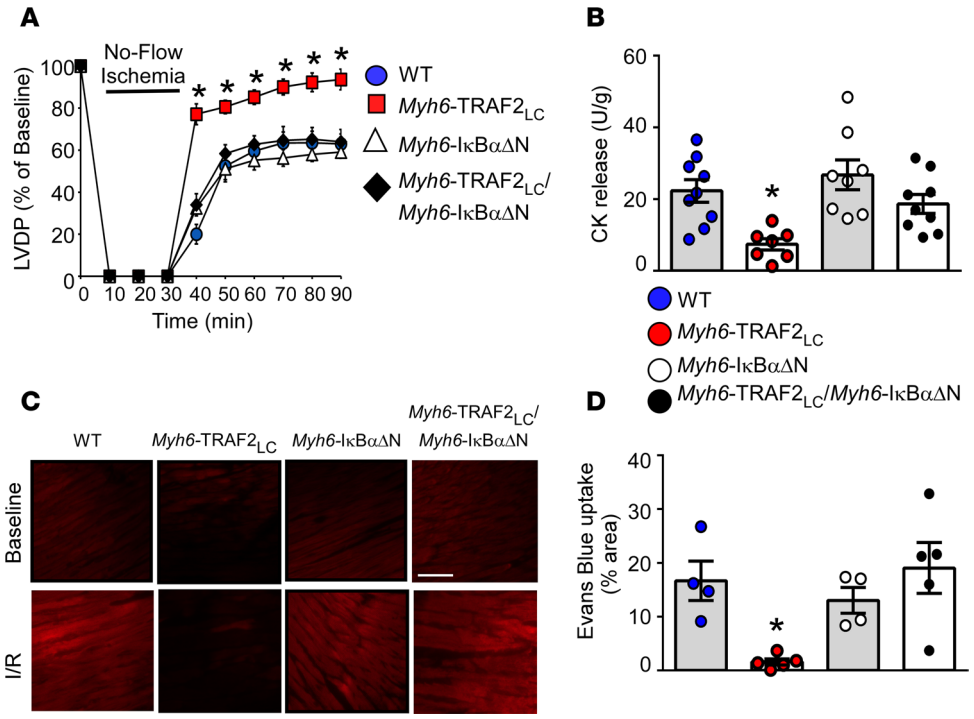

Figure 1. Role of NF-κB signaling in TRAF2-mediated cytoprotection during I/R injury. (**A**) Percent recovery of left ventricular developed pressure (LVDP) following Langendorff perfusion of WT, *Myh6*-TRAF2$_{LC}$, *Myh6*-IκBαΔN, and *Myh6*-TRAF2$_{LC}$/*Myh6*-IκBαΔN mouse hearts (n = 5–6/group) (*P < 0.05 compared with WT by repeated measures analysis using mixed models methodology). (**B**) Creatine kinase (CK) release measured in the effluent following 30 minutes of reperfusion (n = 7–9/group). (**C**) Representative images of Evans blue dye (EBD) uptake (scale bar: 50 μm) (data is representative of 4 independent experiments). (**D**) Group data for EBD uptake as percent area (n = 4–5/group) (*P < 0.05 by 1-way ANOVA compared with WT controls). Data are presented as mean ± SEM.

at least in part, through upregulation of cytoprotective or structural genes downstream from NF-κB signaling (13, 14). In subsequent studies, we showed that TNF/TRAF2-mediated signaling is cytoprotective through a potentially novel E3 ligase–dependent pathway that enables increased mitochondrial autophagy in cardiac myocytes (11). A recent study has also shown that genetic deletion of TRAF2 triggers necroptotic cell death through an NF-κB–independent pathway (10). In order to further explore the contribution of NF-κB–dependent cytoprotective effects of TRAF2, we employed genetic gain- and loss-of-function studies ex vivo and in vivo. Here, we show the finding that RelB, a member of the NF-κB2 family of transcription factors involved in noncanonical NF-κB signaling, is upregulated by TRAF2 and is required for mediating the cytoprotective effects of TRAF2 overexpression. We further show that the cytoprotective effects of TRAF2 are mediated by crosstalk between the canonical and noncanonical NF-κB signaling pathways, thereby revealing a complexity for NF-κB signaling in the heart.

Results

Role of NF-κB signaling in the cytoprotective effects of TRAF2. To determine whether the cardioprotective effects of TRAF2 were mediated through an NF-κB–dependent pathway, we crossed mice overexpressing TRAF2 under the control of the *Myh6* promoter (*Myh6*-TRAF2$_{LC}$) with mice overexpressing a mutated IκBα (IκBαΔN) under the control of the *Myh6* promoter (*Myh6*-IκBαΔN), to generate a line of *Myh6*-TRAF2$_{LC}$/*Myh6*-IκBαΔN double-transgenic mice. The baseline cardiac phenotype was not significantly different among 12-week-old WT, *Myh6*-IκBαΔN, and *Myh6*-TRAF2$_{LC}$/*Myh6*-IκBαΔN mice (Supplemental Figure 1; supplemental material available online with this article; https://doi.org/10.1172/jci.insight.98278DS1). Mouse hearts were subjected to 30 minutes of no-flow ischemia, followed by 60 minutes of reperfusion ex vivo. Figure 1A shows that *Myh6*-TRAF2$_{LC}$ mouse hearts had significantly improved recovery of LV function (P < 0.001 overall) when compared with WT mouse hearts, as we have reported previously (9, 13). Strikingly, the cytoprotective effects of TRAF2 were completely abrogated in the *Myh6*-TRAF2$_{LC}$/*Myh6*-IκBαΔN double-transgenic mice (P > 0.99 overall compared with WT). Of note, the degree of recovery of LV function

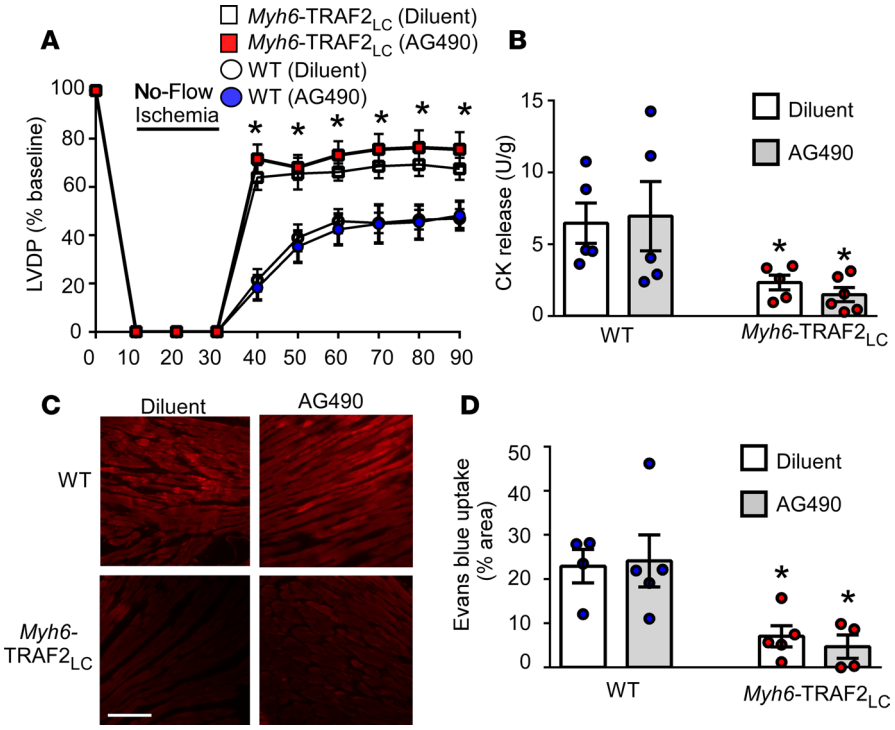

Figure 2. Role of JAK/STAT pathway in mediating the protective effects of TRAF2 during I/R injury. (**A**) Percent recovery of left ventricular developed pressure (LVDP) in the presence of 10 μM AG490 or diluent control in WT and *Myh6*-TRAF2$_{LC}$ mouse hearts (n = 5–7/group) (*P < 0.05 compared with WT by repeated measures analysis using mixed models methodology). (**B**) Creatine kinase (CK) release measured in the effluent following 30 minutes of reperfusion (n = 5–6/group). (**C**) Representative images of Evans Blue dye (EBD) uptake (scale bar: 100 μm) (data is representative of 4 independent experiments). (**D**) Group data for EBD uptake (n = 4–5/group) (*P < 0.05 by 2-tailed t test compared with diluent controls). Data are presented as mean ± SEM.

was not significantly (P > 0.99) different in the *Myh6*-IκBαΔN mice when compared with the WT mice. To determine whether the absence of functional recovery in the *Myh6*-TRAF2$_{LC}$/*Myh6*-IκBαΔN double-transgenic mouse hearts was the result of increased myocyte injury, we measured creatine kinase (CK) release and Evans blue dye (EBD) uptake. As shown by the group data in Figure 1B, there was significantly decreased CK release (P = 0.008) after I/R injury in the *Myh6*-TRAF2$_{LC}$ mouse hearts when compared with WT; however, the CK release in the double-transgenic *Myh6*-TRAF2$_{LC}$/*Myh6*-IκBαΔN mouse hearts was not significantly different (P > 0.99) from the values in WT mouse hearts. As shown by the representative fluorescence photomicrographs (Figure 1C) and the group data (Figure 1D), there was a significant (P = 0.019) decrease in EBD uptake in the hearts of the *Myh6*-TRAF2$_{LC}$ mice compared with WT hearts 30 minutes after I/R injury, whereas the degree of EBD uptake in the *Myh6*-TRAF2$_{LC}$/*Myh6*-IκBαΔN mouse hearts was not significantly different (P > 0.99) from the values in WT mouse hearts. Viewed together, these results suggest that NF-κB is required for the cardioprotective effects of TRAF2.

Role of JAK/STAT signaling on the cytoprotective effects of TRAF2. Previous studies have suggested that the cytoprotective effects of TNF are mediated through the SAFE pathway, insofar as TNF-induced preconditioning was sensitive to pharmacologic inhibition of the JAK/STAT pathway (15, 16). To determine whether STAT3 was involved in the cytoprotective effects of TRAF2, we performed I/R injury experiments ex vivo in the presence or absence of AG490, an inhibitor of STAT3 phosphorylation. As shown in Supplemental Figure 2, there was increased phosphorylation of STAT3 in the nucleus of the diluent treated *Myh6*-TRAF2$_{LC}$ mouse hearts when compared with diluent-treated WT mouse hearts, which was attenuated by 10 μM AG490 (P = 0.033 compared with diluent treated *Myh6*-TRAF2$_{LC}$ mouse hearts), consistent with prior reports (15). However, recovery of LV-developed pressure following I/R injury was not significantly attenuated in the AG490-treated *Myh6*-TRAF2$_{LC}$ mouse hearts (P = 0.96 overall) when compared with diluent-treated *Myh6*-TRAF2$_{LC}$ mouse hearts (Figure 2A). Moreover, the TRAF2-mediated decrease in CK release and decrease in EBD uptake in the *Myh6*-TRAF2$_{LC}$ mouse hearts was not attenuated (P = 0.27 for CK and P = 0.54 for EBD) by treatment with AG490 (Figures 2, B–D). Viewed together, these

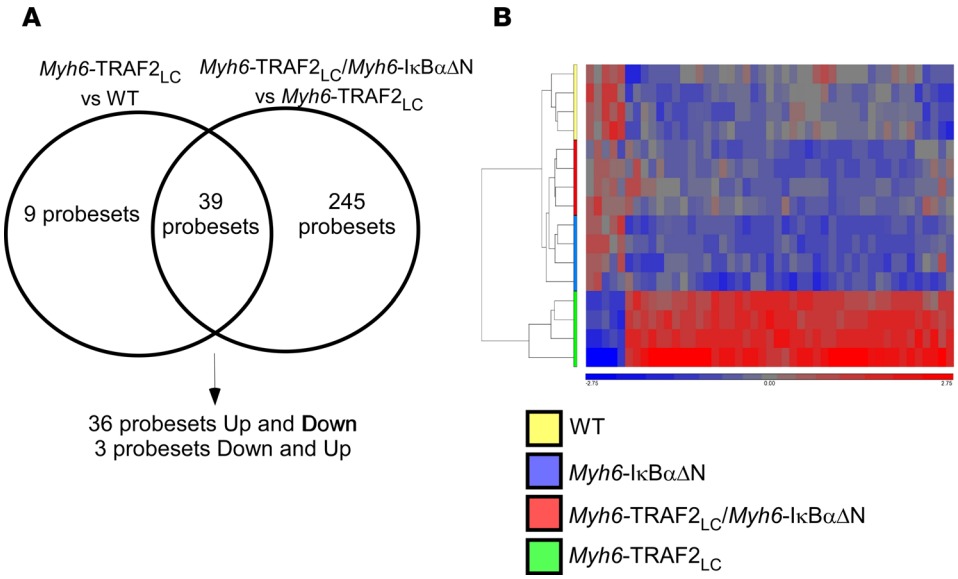

Figure 3. Transcriptional profiling of WT, *Myh6*-TRAF2$_{LC}$, and *Myh6*-TRAF2$_{LC}$/*Myh6*-IκBαΔN mice. (**A**) Venn diagram of genes differentially regulated (absolute fold-change ≥ 1.2, FDR < 0.05) in *Myh6*-TRAF2$_{LC}$ vs. WT, and *Myh6*-TRAF2$_{LC}$/*Myh6*-IκBαΔN vs. *Myh6*-TRAF2$_{LC}$ mice (n = 4/group); the overlap shows genes that are regulated in opposite directions. (**B**) Hierarchical clustering based on significantly different genes in *Myh6*-TRAF2$_{LC}$ vs. WT mouse hearts.

results suggest that, while STAT3 is activated in the hearts of *Myh6*-TRAF2$_{LC}$ mice, STAT3 signaling is not required for the cytoprotective effects of TRAF2 in the heart.

Transcriptional profiling of Myh6-TRAF2$_{LC}$ and Myh6-TRAF2$_{LC}$/Myh6-IκBαΔN mouse hearts. To explore the potential mechanisms responsible for the NF-κB–mediated cytoprotective effects of TRAF2, we performed transcriptional profiling in 12-week-old naive WT, *Myh6*-TRAF2$_{LC}$, *Myh6*-IκBαΔN, and *Myh6*-TRAF2$_{LC}$/*Myh6*-IκBαΔN mouse hearts. Figure 3A shows that there were 48 probe sets that were differentially regulated in the *Myh6*-TRAF2$_{LC}$ vs. WT mouse hearts and 284 probe sets that were differentially regulated in the *Myh6*-TRAF2$_{LC}$ vs. *Myh6*-TRAF2$_{LC}$/*Myh6*-IκBαΔN mouse hearts. The salient finding shown by the Venn diagrams in Figure 3A is that, of the 48 probe sets that were differentially regulated in the *Myh6*-TRAF2$_{LC}$ vs. WT mouse hearts, 39 probe sets were normalized in the *Myh6*-TRAF2$_{LC}$/*Myh6*-IκBαΔN mouse hearts (36 probes up and down and 3 probes down and up), suggesting that NF-κB–mediated signaling was responsible for the majority of the changes in gene expression observed in the *Myh6*-TRAF2$_{LC}$ mouse hearts. Agglomerative hierarchical clustering of the expression of these 48 probe sets showed that *Myh6*-TRAF2$_{LC}$ mouse hearts clustered separately, whereas *Myh6*-IκBαΔN and *Myh6*-TRAF2$_{LC}$/*Myh6*-IκBαΔN mouse hearts clustered with WT mouse hearts (Figure 3B), further suggesting that the differences in gene expression in the *Myh6*-TRAF2$_{LC}$ mouse hearts was mediated through NF-κB signaling. While the number of mRNAs that were normalized in the *Myh6*-TRAF2$_{LC}$/*Myh6*-IκBαΔN mouse hearts was too small to permit typical Gene Ontology or pathway interrogation, inspection of the gene lists (Supplemental Table 1) revealed that there were several genes involved in suppressing the canonical NF-κB signaling (*Tnip1* [FDR < 0.05] and *Nfkbie* [FDR < 0.20]), as well as several genes that were involved in upregulating noncanonical NF-κB signaling (*Relb* [FDR < 0.05], *Traf3* [FDR < 0.05]).

Activation of NF-κB signaling. To further interrogate the potential mechanism(s) through which NF-κB mediates the cytoprotective effects of TRAF2, we performed Western blotting for the NF-κB family member proteins p50, p65, p52, and RelB on nuclear and cytoplasmic extracts from naive 12-week-old WT, *Myh6*-TRAF2$_{LC}$, and *Myh6*-TRAF2$_{LC}$/*Myh6*-IκBαΔN mouse hearts. The important finding shown by Figure 4, A and B, is that the expression of NF-κB family members that are traditionally associated with noncanonical NF-κB signaling, namely p52 and RelB, was significantly increased in the nucleus (P = 0.008 for RelB, P = 0.035 for p52) and cytoplasm (P = 0.009 for RelB, P = 0.026 for p52) of *Myh6*-TRAF2$_{LC}$ mouse hearts when compared with WT mouse hearts; however, there was no significant increase in p50 and p65 subunits in the nucleus (P = 0.89 for p50, P = 0.45 for p65) or cytoplasm (P = 0.63 for p50, P = 0.06 for p65) of *Myh6*-TRAF2$_{LC}$ mouse hearts when compared with WT mouse hearts, which are the subunits traditionally associated with canonical NF-κB signaling. Importantly, the expression of p52 and RelB subunits in

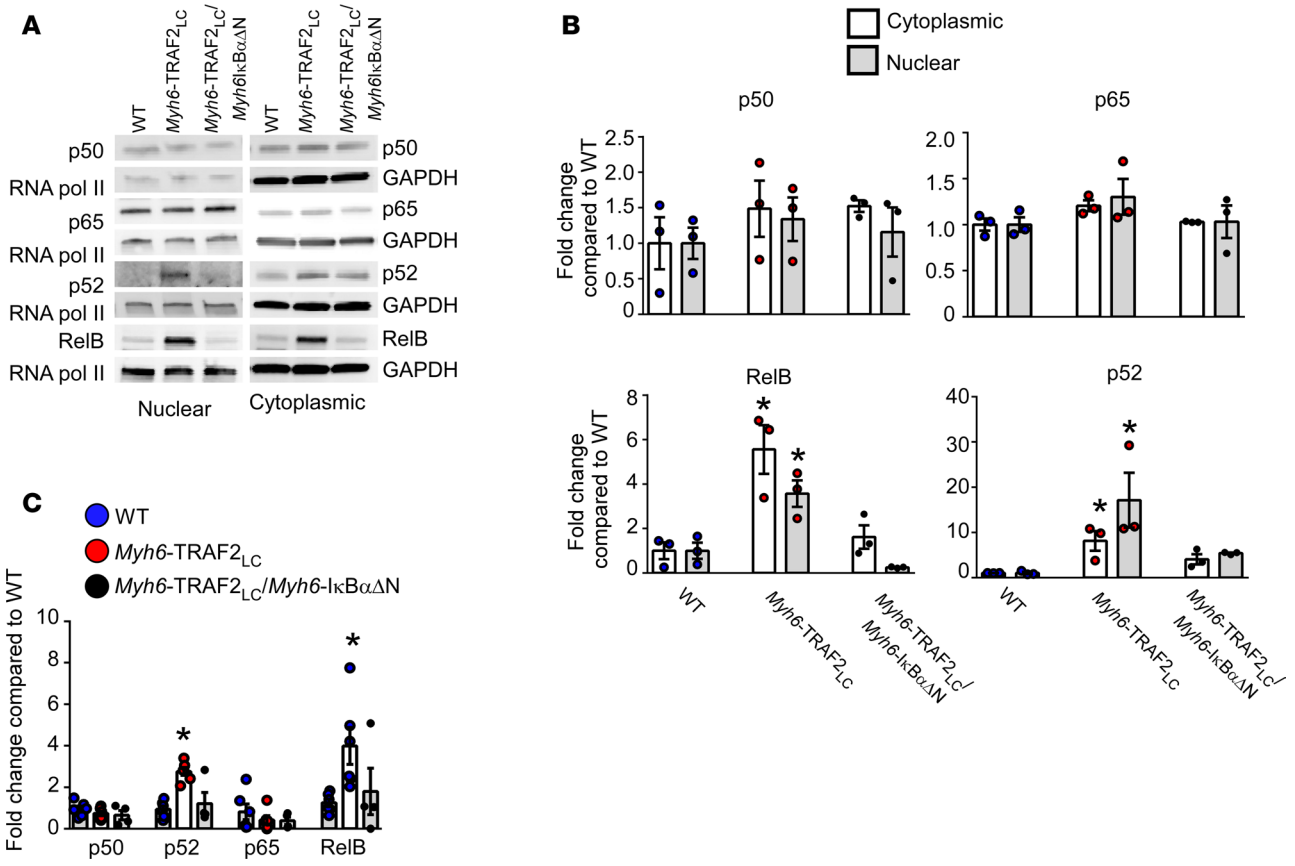

Figure 4. Activation of NF-κB signaling. (**A**) Western blot analysis of NF-κB family members (representative images of 3 independent experiments). (**B**) Quantification of grouped Western blot data (n = 3–4/group). (**C**) NF-κB family ELISA (n = 4–7/group). (*P < 0.05 by 1-way ANOVA compared with WT controls). Data are presented as mean ± SEM.

the nuclear (P = 0.82 for p52, P = 0.48 for RelB) and cytosolic extracts (P = 0.38 for p52, P > 0.99 for RelB) from the *Myh6*-TRAF2$_{LC}$/*Myh6*-IκBαΔN mouse hearts was not significantly different from values in WT mouse hearts. The functional activity of p50, p65, p52, and RelB subunits was evaluated using a DNA-binding ELISA. Figure 4C shows that there was significantly increased binding of p52 (P < 0.001) and RelB (P = 0.022) to NF-κB consensus oligonucleotides in the nuclear extracts from *Myh6*-TRAF2$_{LC}$ mouse hearts when compared with WT, which was significantly attenuated in the *Myh6*-TRAF2$_{LC}$/*Myh6*-IκBαΔN mouse hearts (P > 0.99 compared with WT). There was, however, no increase in binding of canonical NF-κB family members, p50 (P = 0.41) and p65 (P = 0.34), in the *Myh6*-TRAF2$_{LC}$ mouse hearts, consistent with our prior study (17). Viewed together, these results suggest that TRAF2 overexpression leads to activation of noncanonical NF-κB signaling that is mediated via the canonical NF-κB signaling pathway.

Noncanonical NF-κB signaling in Myh6-TRAF2$_{LC}$ mouse hearts. NF-κB–inducing kinase (NIK; MAP3K) is a central signaling component of the noncanonical NF-κB pathway. Under normal conditions NIK proteins are kept at low levels through continuous degradation mediated by TRAF2 and TRAF3 (18). If NIK is allowed to accumulate, it initiates IKKα-mediated phosphorylation of p100, resulting in partial proteosomal degradation of p100 and release of p52 (the N-terminus of p100), which preferentially complexes with RelB and translocates to the nucleus. As shown in Supplemental Figure 3A, NIK was not detectable in the cytosolic extracts from WT, *Myh6*-TRAF2$_{LC}$, *Myh6*-IκBαΔN, or *Myh6*-TRAF2$_{LC}$/*Myh6*-IκBαΔN mouse hearts, despite using an antibody that was able to detect a transfected NIK construct. Supplemental Figure 3B shows that there was increased p100 translocation to the nucleus, a feature of constitutive p100 processing (19), as well as increased constitutive processing of p100 to p52 in cytosolic and nuclear extracts of *Myh6*-TRAF2$_{LC}$ mouse hearts when compared with WT and *Myh6*-TRAF2$_{LC}$/*Myh6*-IκBαΔN mouse hearts (Supplemental Figure 3B). Viewed together, these observations are consistent with increased activation of the noncanonical NF-κB signaling pathway in the *Myh6*-TRAF2$_{LC}$ mouse hearts.

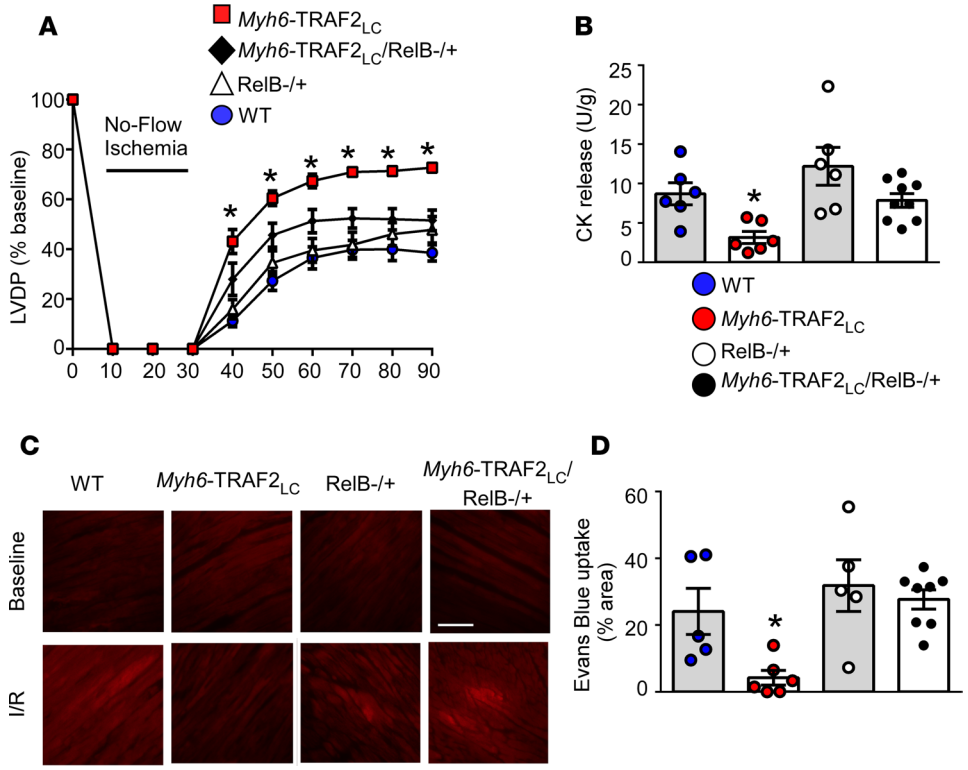

Figure 5. Role of RelB in the mediating the protective effects of TRAF2 during I/R injury. (**A**) Percent recovery of LVDP following I/R injury of WT, *Myh6*-TRAF2$_{LC}$, RelB$^{-/+}$, and *Myh6*-TRAF2$_{LC}$/RelB$^{-/+}$ (n = 9–13/group) mouse hearts (*P < 0.05 compared with WT controls by repeated measures analysis using mixed models methodology). (**B**) Creatine kinase (CK) release measured in the effluent following 30 minutes of reperfusion (n = 6–9/group). (**C**) Representative images Evans Blue dye (EBD) uptake (scale bar: 50 μm) (data are representative of 6 independent experiments). (**D**) Group data for EBD uptake (n = 5–9/group) (*P < 0.05 by 1-way ANOVA compared with WT controls). Data are presented as mean ± SEM.

Role of RelB in mediating the cytoprotective effects of TRAF2. To explore the contribution of RelB to the cytoprotective phenotype observed in the *Myh6*-TRAF2$_{LC}$ mouse hearts, we crossed RelB$^{-/+}$ mice with *Myh6*-TRAF2$_{LC}$ mice and then performed I/R injury both ex vivo and in vivo. The baseline cardiac phenotype of the RelB$^{-/+}$ and *Myh6*-TRAF2$_{LC}$/RelB$^{-/+}$ mice was not significantly different from WT mice at 12 weeks of age (Supplemental Figure 4), with the exception that the percent fractional shortening (%FS) was significantly (P = 0.025) reduced, and the heart weight–to–body weight ratio (HW/BW) was significantly increased (P = 0.009) in the *Myh6*-TRAF2$_{LC}$/RelB$^{-/+}$ mice compared with WT, consistent with our prior observation that %FS is slightly decreased and the HW/BW slightly increased in *Myh6*-TRAF2$_{LC}$ mouse hearts (9). Despite these alterations in %FS and HW/BW, *Myh6*-TRAF2$_{LC}$ mice had a cytoprotective phenotype. To determine the functional effects of RelB signaling, hearts from WT, *Myh6*-TRAF2$_{LC}$, RelB$^{-/+}$, and *Myh6*-TRAF2$_{LC}$/RelB$^{-/+}$ mice were subjected to 30 minutes of no-flow ischemia, followed by 60 minutes of reperfusion ex vivo. Figure 5A, shows that the degree of functional recovery of the RelB$^{-/+}$ heterozygous mice was not significantly different (P = 0.962 overall) from WT mice. However, the salient finding shown by Figure 5A is that the improved recovery of LV function observed in the *Myh6*-TRAF2$_{LC}$ mouse hearts relative to WT mouse hearts (P < 0.001 overall) was not evident in the *Myh6*-TRAF2$_{LC}$/RelB$^{-/+}$ mouse hearts, which were not significantly different from WT mouse hearts (P = 0.064). To determine whether the loss of functional recovery in the *Myh6*-TRAF2$_{LC}$/RelB$^{-/+}$ mouse hearts was the result of increased myocyte injury, we measured CK release and EBD uptake. As shown by the group data for CK in Figure 5B and the EBD uptake in Figure 5, C and D, the significant decrease in CK release (P = 0.044) and EBD (P = 0.029) uptake observed in the *Myh6*-TRAF2$_{LC}$ mouse hearts relative to WT mouse hearts was completely abrogated in the *Myh6*-TRAF2$_{LC}$/RelB$^{-/+}$ mouse hearts. The degree of CK release and EBD uptake was not significantly different from WT controls in the RelB$^{-/+}$ mice (P = 0.334 for CK, P = 0.891 for EBD) or the *Myh6*-TRAF2$_{LC}$/RelB$^{-/+}$ mouse hearts (P > 0.99 for CK, P > 0.99 for EBD).

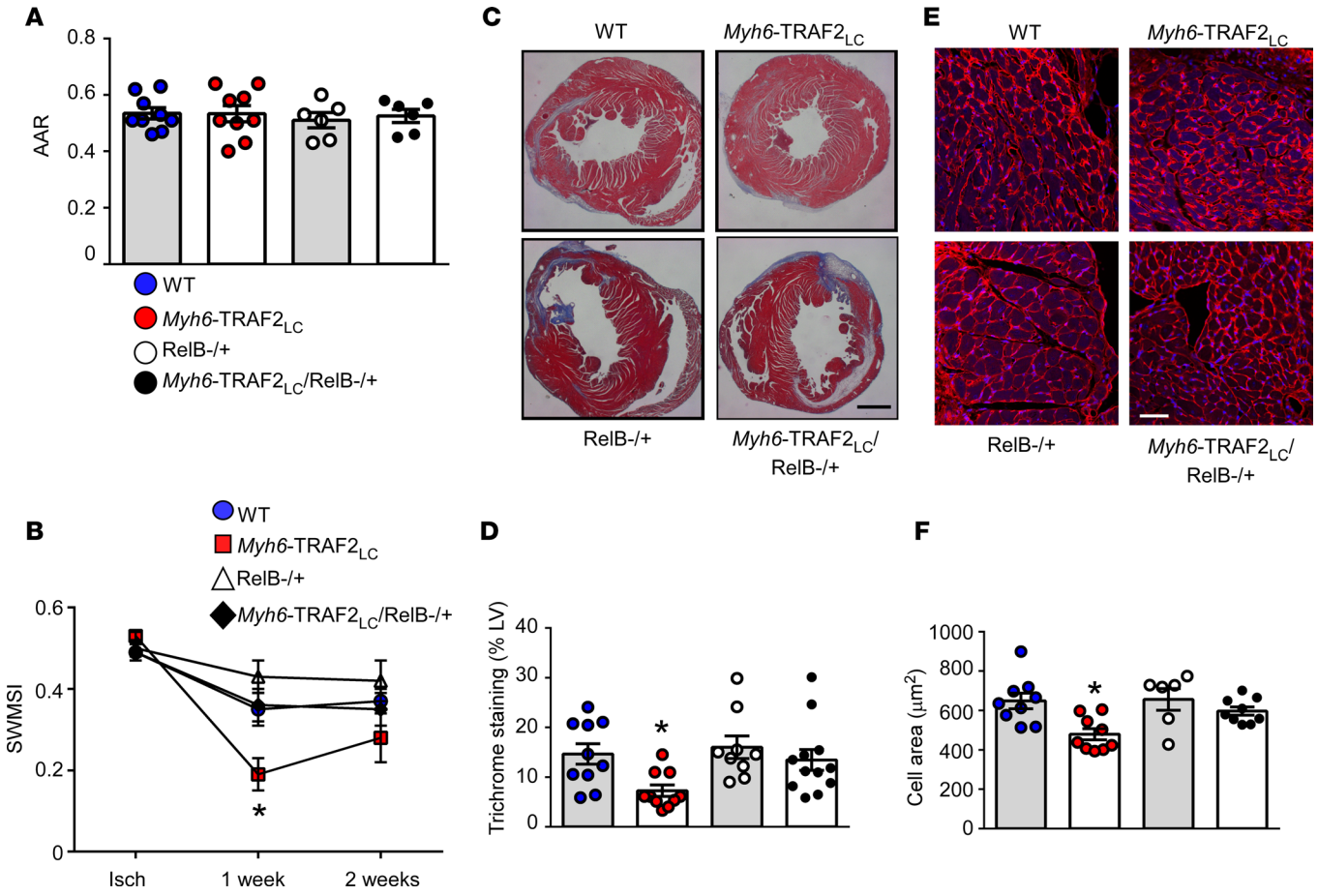

Figure 6. In vivo closed-chest I/R in WT, *Myh6*-TRAF2$_{LC}$, RelB$^{-/+}$, *Myh6*-TRAF2$_{LC}$/RelB$^{-/+}$ mice. (**A**) Area-at-risk (AAR) (n = 6–9 per group) (*P < 0.05 by 1-way ANOVA compared with WT controls). (**B**) Segmental Wall Motion Score Index (SWMSI) (n = 6–10 per group) (*P < 0.05 compared with WT by repeated measures analysis using mixed models methodology). (**C**) Masson's trichrome staining (scale bar: 1 mm) (representative images of 7 independent experiments). (**D**) Quantification of group data for Masson's trichrome staining (n = 10–12/group). (**E**) Representative images of wheat germ agglutinin (WGA) staining (scale bar: 50 μm) (data are representative of 3 independent experiments). (**F**) Group data of cardiac myocyte cell size based on WGA staining (n = 20 cells counted/section, 3 sections per heart, 3 mouse hearts per group) (*P < 0.05 by 1-way ANOVA compared with WT controls). Data are presented as mean ± SEM.

To further explore the role of RelB in terms of mediating the cytoprotective effects of TRAF2, we performed closed-chest I/R studies in WT, *Myh6*-TRAF2$_{LC}$, RelB$^{-/+}$, and *Myh6*-TRAF2$_{LC}$/RelB$^{-/+}$ mice using 90 minutes of ischemia, followed by 2 weeks of reperfusion, as described (20). Figure 6A shows that there was no significant difference (P = 0.87 overall) in the area at risk in each of the 4 groups of mice at the time of reperfusion. Figure 6B shows that the segmental wall motion score index (SWMSI), a noninvasive measurement of infarct size (21), was significantly less (P = 0.028) for the *Myh6*-TRAF2$_{LC}$ mice when compared with WT mice 1 week after I/R injury in vivo. Although the SWMSI was numerically increased at 2 weeks in the *Myh6*-TRAF2$_{LC}$ mice, these values were not significantly different (P = 0.1) from the values at 1 week. However, the SWMSI at 1 week was not significantly different in the RelB$^{-/+}$ (P = 0.824) and *Myh6*-TRAF2$_{LC}$/RelB$^{-/+}$ (P > 0.99) mouse hearts when compared with WT mice. Two weeks after I/R injury, there was no significant difference in the LV end-diastolic volume, LV end-systolic volume, LV ejection fraction, or HW/BW ratio between the WT, *Myh6*-TRAF2$_{LC}$, RelB$^{-/+}$, or *Myh6*-TRAF2$_{LC}$/RelB$^{-/+}$ mouse hearts (Supplemental Figure 5).

Hearts were harvested and analyzed for fibrosis, using Masson's trichrome staining (Figure 6, C and D) and Picrosirius red staining (Supplemental Figure 5), and the myocyte cross-sectional area was measured by staining with wheat germ agglutinin (WGA) (Figure 6, E and F). There was a significant decrease in trichrome staining (P = 0.0085; Figure 6, C and D) and Picrosirius red staining (P = 0.0406; Supplemental Figure 5) in the *Myh6*-TRAF2$_{LC}$ mouse hearts compared with WT mouse hearts; however, the degree of

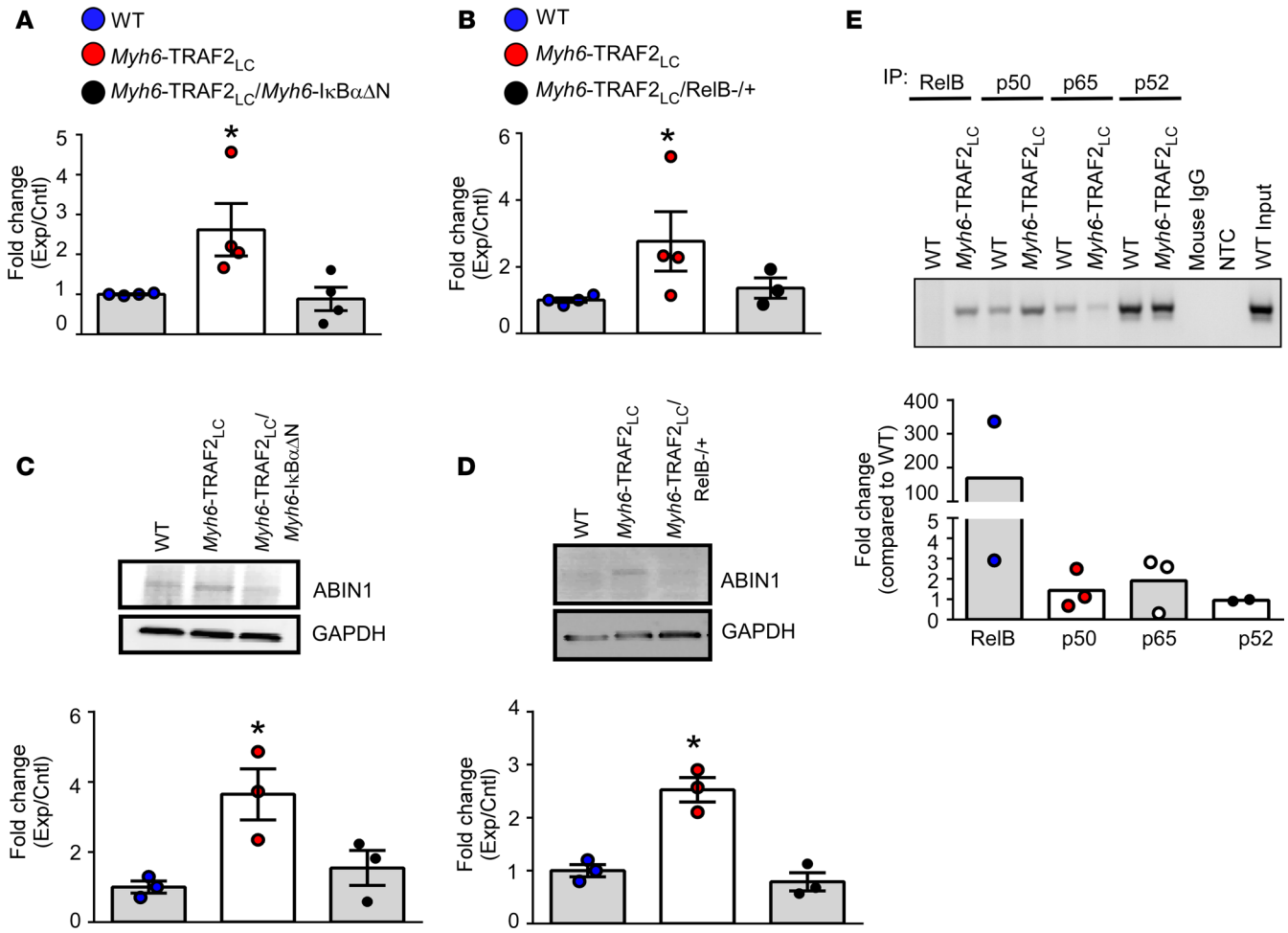

Figure 7. TRAF2-mediated upregulation of ABIN-1. (**A**) qPCR quantification of *Tnip1* (gene name for ABIN1 protein) in WT, *Myh6*-TRAF2$_{LC}$, and *Myh6*-TRAF2$_{LC}$/*Myh6*-IκBαΔN mouse hearts (n = 4/group). (**B**) qPCR quantification of *Tnip1* in WT, *Myh6*-TRAF2$_{LC}$, and *Myh6*-TRAF2$_{LC}$/RelB$^{-/+}$ mouse hearts (n = 3–4/group). (**C**) Western blot analysis of ABIN1 in WT, *Myh6*-TRAF2$_{LC}$, and *Myh6*-TRAF2$_{LC}$/*Myh6*-IκBαΔN mouse hearts (n = 3/group). (**D**) Western blot analysis of ABIN1 in WT, *Myh6*-TRAF2$_{LC}$, and *Myh6*-TRAF2$_{LC}$/RelB$^{-/+}$ mouse hearts (n = 3/group). (**E**) ChIP assay of *Tnip1* promoter using antibodies to members of the NF-κB family (n = 3/group) (*P < 0.05 by 1-way ANOVA compared with WT controls). Data are presented as mean ± SEM.

Masson's trichrome staining and Picrosirius red staining was not different in the RelB$^{-/+}$ (P > 0.99 for trichrome and Picrosirius red) or *Myh6*-TRAF2$_{LC}$/RelB$^{-/+}$ (P > 0.99 for trichrome and Picrosirius red) mouse hearts when compared with WT mouse hearts. Figure 6E shows representative WGA staining of myocyte cross-sectional area in the periinfarct zone in WT, *Myh6*-TRAF2$_{LC}$, RelB$^{-/+}$, or *Myh6*-TRAF2$_{LC}$/RelB$^{-/+}$ mouse hearts, whereas Figure 6F summarizes the results of group data. As shown, myocyte cross-sectional area was significantly (P < 0.0001) less in the *Myh6*-TRAF2$_{LC}$ mouse hearts when compared with WT mouse hearts. Importantly, myocyte cross-sectional area was not significantly different in the RelB$^{-/+}$ (P > 0.99) or *Myh6*-TRAF2$_{LC}$/RelB$^{-/+}$ (P = 0.12) mouse hearts relative to WT mouse hearts, suggesting that the protective effects of TRAF2 were abrogated in mouse hearts that were haploinsufficient for RelB.

Transcriptional targets of TRAF2-mediated NF-κB signaling. Several downstream NF-κB targets of TRAF2 were identified by microarray analysis (Supplemental Table 1). One of the genes that was differentially regulated in the *Myh6*-TRAF2$_{LC}$ and *Myh6*-TRAF2$_{LC}$/*Myh6*-IκBαΔN mouse hearts was TNFAIP3-interacting protein 1 (*Tnip1*). *Tnip1* codes for ABIN-1, which is a family member of the A20 binding inhibitors of NF-κB and apoptosis signaling (ABIN). ABINs bind to the ubiquitin-editing NF-κB inhibitor protein A20 (TNF-induced protein 3; TNFAIP3) and thus serve as negative feedback inhibitors of canonical NF-κB–mediated signaling (22). Given that canonical NF-kB–mediated signaling was suppressed in the *Myh6*-TRAF2$_{LC}$ mouse hearts, we asked whether noncanonical NF-kB signaling contributed to the observed increased in *Tnip1* expression in *Myh6*-TRAF2$_{LC}$ mouse hearts. We first confirmed the results of

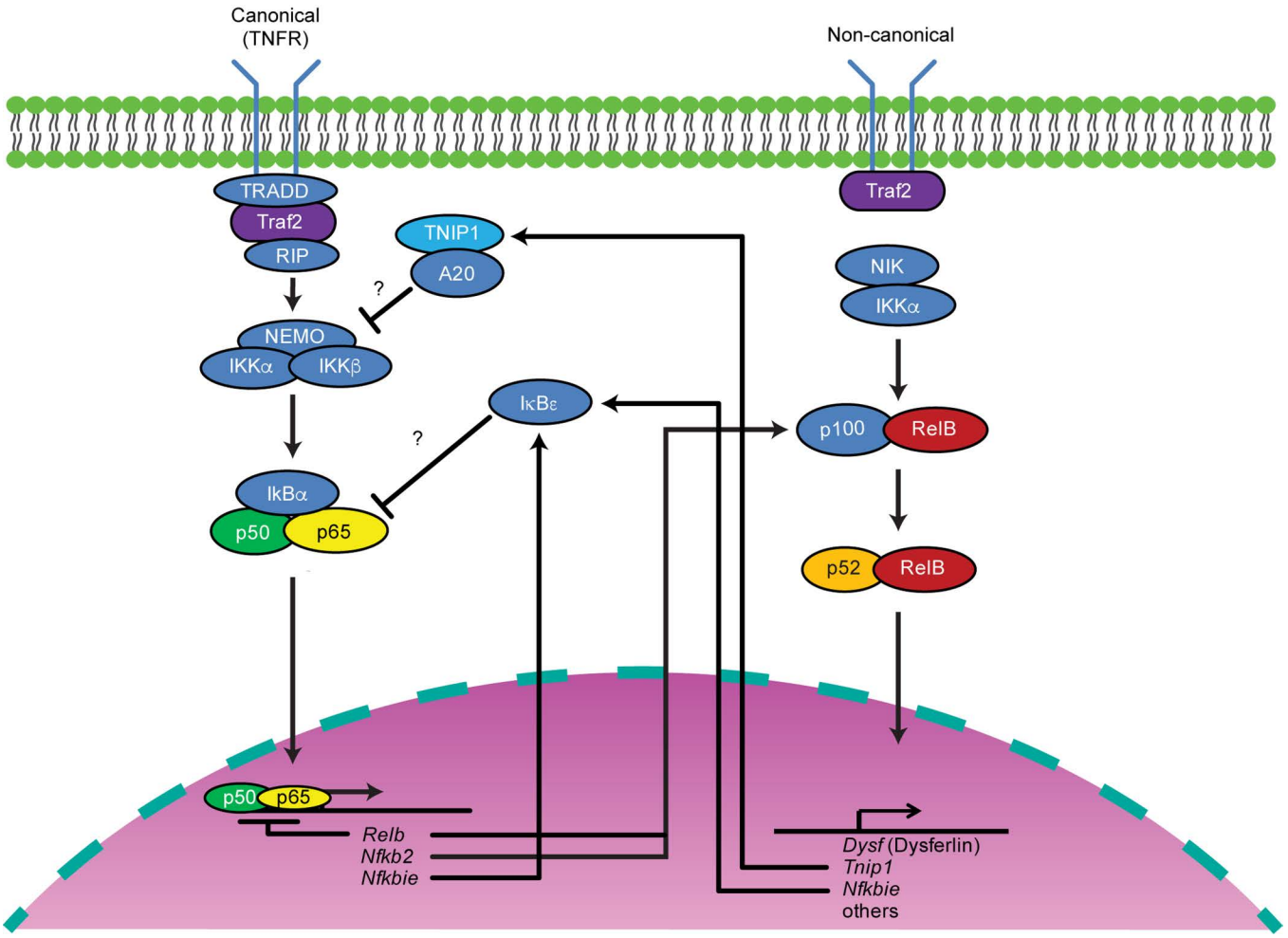

Figure 8. Proposed model for TRAF2-mediated crosstalk between canonical noncanonical NF-κB–mediated signaling pathways. TRADD, TNF receptor type 1–associated DEATH domain protein; RIP, receptor-interacting protein kinase; TRAF2, TNF receptor–associated factor 2; TNIP1, TNFAIP3-interacting protein 1; NEMO, NF-κB essential modulator; IKKα, inhibitor of NF-κB kinase subunit α; IKKβ, inhibitor of NF-κB kinase subunit β; IκBα, NF-κB inhibitor α, NIK, NF-κβ–inducing kinase (also known as MAPK kinase kinase 14; MAP3K14); NFKBIE, NF-κB inhibitor epsilon; IκBε, NF-κB inhibitor ε.

the microarray analysis by quantitative PCR (qPCR) and Western blot analysis in the WT, *Myh6*-TRAF2$_{LC}$, *Myh6*-TRAF2$_{LC}$/*Myh6*-IκBαΔN, and *Myh6*-TRAF2$_{LC}$/RelB$^{-/+}$ mouse hearts. As shown in Figure 7, mRNA levels of *Tnip1* were significantly increased ($P = 0.045$) in *Myh6*-TRAF2$_{LC}$ mouse hearts when compared with WT mouse hearts, whereas the level of expression of *Tnip1* mRNA in *Myh6*-TRAF2$_{LC}$/*Myh6*-IkBαΔN mice (Figure 7A) and *Myh6*-TRAF2$_{LC}$/RelB$^{-/+}$ (Figure 7B) mouse hearts was not significantly different from WT mice ($P > 0.99$ for both). Importantly, Western blot analysis demonstrated that protein levels of ABIN-1 were significantly upregulated ($P = 0.022$) in the *Myh6*-TRAF2$_{LC}$ mouse hearts relative to WT (Figures 7, C and D), whereas ABIN-1 protein levels were not significantly elevated in the *Myh6*-TRAF2$_{LC}$/*Myh6*-IκBαΔN mice (Figure 7C) and *Myh6*-TRAF2$_{LC}$/RelB$^{-/+}$ (Figure 7D) mouse hearts ($P = 0.9716$ and $P > 0.999$, respectively). To determine whether noncanonical NF-κB signaling was responsible for the observed increased in expression of *Tnip1* in *Myh6*-TRAF2$_{LC}$ mouse hearts, we performed a ChIP assay. As shown in Figure 7E, there was an increase in RelB binding to the *Tnip1* promoter in *Myh6*-TRAF2$_{LC}$ mouse hearts, whereas RelB binding was not detected in the WT mouse hearts. In contrast, the levels of p50, p52, and p65 binding to the *Tnip1* promoter were relatively unchanged in the *Myh6*-TRAF2$_{LC}$ and WT mouse hearts. Although *Nfkbie* was not identified in our microarray analysis using an FDR < 0.05, when we used a more relaxed FDR (<0.20), we observed that the expression of *Nfkbie* was also differentially regulated in the *Myh6*-TRAF2$_{LC}$ and *Myh6*-TRAF2$_{LC}$/*Myh6*-IκBαΔN mouse hearts. Supplemental Figure 6 shows that the expression of IκBε (mRNA and protein) was significantly increased in *Myh6*-TRAF2$_{LC}$ mouse hearts when compared with WT mouse hearts, whereas the expression level of IκBε (mRNA and protein) was

normalized in the *Myh6*-TRAF2$_{LC}$/*Myh6*-IκBαΔN mouse hearts. In addition, we detected increased RelB binding to the *Nfkbie* promoter in *Myh6*-TRAF2$_{LC}$ mouse hearts, whereas RelB binding was not detected in the WT mouse hearts. Viewed together, these results implicate an important role for RelB with respect to TRAF2-mediated *Tnip1* and *Nfkbie* gene expression.

Discussion

Although it has long been recognized that activation of the innate immune system confers cytoprotective responses in the heart, the precise mechanisms that are responsible for these beneficial effects are not well known. Here, we show that TRAF-mediated cytoprotective responses in the heart require crosstalk between the canonical and noncanonical NF-κB signaling pathways. Three compelling lines of information support this statement. First, LV functional recovery was significantly improved and the extent of LV tissue injury was significantly less following I/R injury in *Myh6*-TRAF2$_{LC}$ when compared with control mice (Figure 1), consistent with our prior observations (9). Remarkably, the cytoprotective effects of TRAF2 were completely abolished in double-transgenic *Myh6*-TRAF2$_{LC}$/*Myh6*-IκBαΔN mice that lack NF-κB signaling through the canonical pathway (23). To determine whether activation of the SAFE pathway was required for the cytoprotective effects of TRAF2, as has been reported for TNF-mediated preconditioning and/or postconditioning (15, 16), we performed I/R injury ex vivo in the presence or the absence of AG490, a STAT3 inhibitor. Although STAT3 was significantly activated in the *Myh6*-TRAF2$_{LC}$ mouse hearts relative to WT control mice (Supplemental Figure 2), and STAT3 activation was abrogated by treatment with AG490, inhibition of STAT3 did not attenuate the improved recovery of LV function, nor did it attenuate the decrease in LV tissue injury in the *Myh6*-TRAF2$_{LC}$ mouse hearts (Figure 2), suggesting that while STAT3 is activated in *Myh6*-TRAF2$_{LC}$ mouse hearts, it is not required for the cytoprotective effects of TRAF2.

Second, to elucidate the potential mechanism(s) for the NF-κB–mediated cytoprotective effects of TRAF2, we performed Western blotting for NF-κB family members, p65 (RelA), p50, p52, and RelB, as well as DNA binding assays on nuclear extracts from WT, *Myh6*-TRAF2$_{LC}$, *Myh6*-IκBαΔN, or *Myh6*-TRAF2$_{LC}$/*Myh6*-IκBαΔN mouse hearts. We observed increased expression levels and increased DNA binding of NF-κB family members that are traditionally associated with noncanonical NF-κB signaling, namely p52 and RelB (Figure 4), whereas there was no increase in expression or DNA binding of the p50 and p65 subunits, which are traditionally associated with canonical NF-κB signaling. Importantly, the increase in expression and DNA binding of the p52 and RelB subunits in the *Myh6*-TRAF2$_{LC}$ mouse hearts were normalized in *Myh6*-TRAF2$_{LC}$/*Myh6*-IκBαΔN mouse hearts that lacked canonical NF-κB signaling (Figure 4), suggesting that there was crosstalk between the canonical and noncanonical NF-κB pathways (19). Third, to determine whether activation of noncanonical NF-κB signaling was responsible for the observed cytoprotective effects of TRAF2, we performed I/R injury ex vivo and in vivo in *Myh6*-TRAF2$_{LC}$ mice that were haploinsufficient for RelB (*Myh6*-TRAF2$_{LC}$/RelB$^{-/+}$ mice). Figures 5 and 6 show that the improved LV functional recovery in *Myh6*-TRAF2$_{LC}$ mouse hearts was attenuated in the *Myh6*-TRAF2$_{LC}$/RelB$^{-/+}$ mice ex vivo (Figure 5A) and in vivo (Figure 6B). Moreover, the TRAF2-mediated decrease in tissue injury (Figures 5, B–D) and myocardial fibrosis (Figure 6, C and D, and Supplemental Figure 5) observed in the *Myh6*-TRAF2$_{LC}$ mouse hearts was abrogated in the *Myh6*-TRAF2$_{LC}$/RelB$^{-/+}$ mouse hearts. These results, when viewed together, suggest that crosstalk between the canonical and noncanonical NF-κB signaling pathways is required for mediating the cytoprotective effects of TRAF2.

Crosstalk between canonical and noncanonical NF-κB signaling. Activation of NF-κB results in the induction of a panoply of biological responses ranging from cellular stress responses, cell survival, immune responses, and cell maturation. Based on the components of the signaling cascade, NF-κB signaling is broadly categorized into canonical and noncanonical pathways, which are mediated through different cell surface receptors, cytoplasmic adaptors, and NF-κB homo- and heterodimers. Activation of the canonical NF-κB pathway provides rapid responses (within minutes), both in terms of activation and deactivation, and occurs in response to a broad variety of environmental stimuli. In contrast, the noncanonical pathway is comparatively slower (activated within hours) and is more persistent. Although these 2 pathways have been regarded as functionally distinct parallel signaling pathways, more recent studies have shown that there is bidirectional crosstalk between canonical and noncanonical signaling (19).

Here, we show that crosstalk between the canonical and noncanonical NF-κB pathways is responsible for mediating the cytoprotective effects of TRAF2 ex vivo and in vivo, and that this crosstalk occurs at several different interdependent levels, including increased synthesis of RelB, increased processing of p100,

and increased synthesis of proteins that directly inhibit canonical NF-κB signaling (ABIN-1 and IκBε). Our data suggest that canonical NF-κB–induced expression of RelB contributed to activation of noncanonical signaling in the *Myh6*-TRAF2$_{LC}$ mouse hearts, given that the significant increase in RelB expression in the *Myh6*-TRAF2$_{LC}$ mouse hearts was abrogated in the *Myh6*-TRAF2$_{LC}$/*Myh6*-IκBαΔN mouse hearts that lacked canonical NF-κB signaling. Although canonical NF-κB–induced expression of RelB has been reported to promote or inhibit signaling through the noncanonical pathway (19), our results suggest that RelB-mediated activation of noncanonical signaling is required for the cytoprotective effects of TRAF2, insofar as the cytoprotective effects of TRAF2 were absent in mice that were haploinsufficient for RelB signaling. Further, a ChIP assay revealed the presence of RelB on the promoter regions of *Tnip1* and *Nfkbie,* which were upregulated in the *Myh6*-TRAF2$_{LC}$ mouse hearts but not in *Myh6*-TRAF2$_{LC}$/*Myh6*-IκBαΔN mouse hearts, suggesting that NF-κB induction promoted increased RelB-mediated signaling. While we were unable to demonstrate that increased stabilization of NIK was responsible for activation of noncanonical signaling, we did observe increased processing of p100 to p52 in *Myh6*-TRAF2$_{LC}$ mouse hearts (Supplemental Figure 3), consistent with increased NIK signaling. Given that NIK is degraded rapidly, and therefore difficult to detect in vivo, we cannot exclude the formal possibility that NIK stabilization was responsible for the observed increase in p100 processing. The results of this study suggest (but do not prove) that there is a third level of interaction between the canonical and noncanonical signaling pathways in the *Myh6*-TRAF2$_{LC}$ mouse hearts that is mediated by RelB-mediated upregulation of inhibitory proteins that dampen signaling through canonical NF-κB signaling, including ABIN-1 (*Tnip1*). ABIN-1 inhibits canonical NF-κB signaling by physically linking A20 with NEMO, thus facilitating A20-mediated deubiquitination of NEMO-mediated canonical NF-κB signaling (22), increased expression of IκBε — which directly inhibits nuclear translocation of p50 and p65 — and increased nuclear translocation of p100 (IκBδ) — which is able to sequester RelA:p50 homodimers, thereby by dampening canonical NF-κB signaling (24). Additional studies will be required to determine the functional significance of RelB-mediated dampening of canonical NF-κB signaling.

Conclusions. Whereas the role of canonical NF-κB signaling in the heart in response to cardiac injury has been characterized extensively (25), this is the first study to our knowledge to delineate the importance of noncanonical NF-κB signaling in the heart. Here, we suggest that TRAF2 serves as a scaffolding protein that integrates canonical and noncanonical NF-κB signaling in the heart, thereby providing the cardiac myocyte with a broad repertoire of cellular responses to tissue injury, including a brisk inflammatory response mediated by the canonical NF-κB signaling and a slower secondary noncanonical response that is more sustained, and confers cytoprotection by upregulating RelB-dependent cytoprotective genes, as well as by dampening canonical NF-κB signaling, which — if dysregulated — can lead to excessive collateral tissue damage (Figure 8). The observation that sustained TRAF2 signaling conveys cytoprotective responses is consistent with recent clinical observations that have identified TRAF2 as a tumor oncogene and studies that have linked sustained noncanonical NF-κB signaling with cancer initiation and tumor maintenance (26, 27). Although the full ensemble of noncanonical NF-κB–induced cytoprotective genes is not known, we have shown previously that the cytoprotective effects of TRAF2 are mediated, at least in part, by RelB-mediated expression of dysferlin (*Dysf*), which is an "emergency response" gene that facilitates membrane repair (13). Viewed together, these results offer a significant revision of NF-κB signaling in the heart, providing important insights that allow for a reconciliation of the divergent reports of the deleterious and beneficial effects of NF-κB signaling in the heart, and they suggest that a better understanding of how canonical and noncanonical signals are integrated in the heart following tissue injury represents an opportunity for developing novel therapeutic interventions that maximize the beneficial effects of NF-κB signaling without incurring the untoward deleterious effects of dysregulated NF-κB signaling.

Methods

Transgenic mouse lines

The lines of transgenic mice overexpressing TRAF2 and a mutated IκBα (IκBαΔN) transgene under the control of the Myh6 promoter (*Myh6*-TRAF2$_{LC}$ and *Myh6*-IκBαΔN, respectively) have been described previously (9, 23). To determine whether the cardioprotective effects of TRAF2 were mediated through an NF-κB–dependent pathway, we crossed *Myh6*-TRAF2$_{LC}$ mice (FVBN) with *Myh6*-IκBαΔN mice (C57BL/6) to generate *Myh6*-TRAF2$_{LC}$/*Myh6*-IκBαΔN double-transgenic mice. The F1 generation of this cross was

employed in all experiments described herein. RelB-deficient mice were obtained from The Jackson Laboratory (C57BL/6-*Relb*$^{Tg(H2\text{-}K1/GH1)106Bri}$/J) (28) and were outcrossed onto the FVBN background 6 times. In contrast to the homozygous C57BL/6 RelB$^{-/-}$ mice, which develop a wasting syndrome by 3 weeks and die between 3 weeks to several months (28), we observed that the RelB$^{-/-}$ mice bred onto the FVBN background died at approximately 5–6 weeks of age. Therefore, we used FVBN RelB$^{-/+}$ heterozygous mice for all experiments. To determine whether the cardioprotective effects of TRAF2 were mediated through a RelB-dependent pathway, we crossed *Myh6*-TRAF2$_{LC}$ mice (in an FVB/N background) with RelB$^{-/+}$ (in an FVB/N background) mice to generate a line of *Myh6*-TRAF2$_{LC}$/RelB$^{-/+}$ mice. The *Myh6*-TRAF2$_{LC}$/RelB$^{-/+}$ mice were born with the expected Mendelian frequency and had normal life spans. All mice were maintained in a pathogen-free environment and were fed pellet food and water ad libitum.

I/R injury ex vivo

Hearts from 10- to 12-week-old male *Myh6*-TRAF2$_{LC}$, *Myh6*-IκBαΔN, *Myh6*-TRAF2$_{LC}$/*Myh6*-IκBαΔN, RelB$^{-/+}$, and *Myh6*-TRAF2$_{LC}$/RelB$^{-/+}$ mice, and their respective littermate (LM) and/or WT controls, were isolated and perfused at a constant pressure of 70 mm Hg with modified Krebs-Henseleit buffer (MilliporeSigma) as described previously (13). After a 20-minute stabilization period, mouse hearts were subjected to no-flow ischemia (time [t] = 0 minutes) for 30 minutes followed by reperfusion (t = 30 minutes) for up to 60 minutes (t = 90 minutes). To determine whether activation of the STAT3 signaling pathway was responsible for mediating the cytoprotective effects of TRAF2, we treated WT and *Myh6*-TRAF2$_{LC}$ mouse hearts in separate experiments with 10 μM AG490 (MilliporeSigma), a tyrphostin tyrosine kinase inhibitor that blocks signaling through the JAK/STAT pathway, which was added to Krebs-Henseleit buffer (MilliporeSigma) or an equivalent volume of diluent (0.06% ethanol). Mouse hearts were treated for 15 minutes following the 20-minute stabilization period and during the first 15 minutes of the reperfusion period.

Assessment of cardiac myocyte injury after I/R injury

To assess the degree of myocyte injury after I/R injury ex vivo, we assessed CK release in the effluent 30 minutes after reperfusion in 10- to 12-week-old male WT, *Myh6*-TRAF2$_{LC}$, *Myh6*-IκBαΔN, *Myh6*-TRAF2$_{LC}$/*Myh6*-IκBαΔN, RelB$^{-/+}$, and *Myh6*-TRAF2$_{LC}$/RelB$^{-/+}$ mouse hearts, as previously described (9). CK activity was normalized for dry heart weight, and data were expressed as units per gram of cardiac tissue. Because triphenyltetrazolium chloride staining may underestimate the true extent of tissue injury within the first 3 hours of cardiac injury (29), we used EBD (MilliporeSigma) uptake to assess the degree of myocardial tissue injury after I/R injury, as described (9, 13). Mouse hearts were examined at the level of the papillary muscle using a total of 15 microscopic fields per heart. Data are expressed as the percent area of the myocardium with red fluorescence.

I/R injury in vivo

Hearts from WT, *Myh6*-TRAF2$_{LC}$, RelB$^{-/+}$, and *Myh6*-TRAF2$_{LC}$/RelB$^{-/+}$ were subjected to I/R injury, using the closed-chest I/R model developed by Entman and colleagues (30), and modified as we have described previously (31). For the studies described herein, we used 10- to 12-week-old male mice that were anesthetized with 1.5% isoflurane and were then subjected to 90 minutes of closed-chest ischemia, followed by reperfusion for 2 weeks. Sham-operated animals underwent the identical procedure, with the exception that ischemia was not induced.

Echocardiographic studies

Image acquisition. Ultrasound examination of the cardiovascular system was performed using a Vevo 2100 Ultrasound System (VisualSonics Inc.) equipped with a 30 MHz linear-array transducer, as previously described (31).

Imaging protocol. Mice were imaged by echocardiography at 1 day, 1 week, and 2 weeks after I/R injury to evaluate LV structure and function, as described (32).

Quantification of area at risk and infarct size. Noninvasive evaluation of area at risk and infarct size was performed as described using the SWMSI (33). The SWMSI represents the sum of the abnormal segments of the LV wall motion obtained from serial short-axis views divided by the total number of segments of the LV wall (values very from 0–1). Prior studies have shown that SWMSI correlates with acute and chronic infarct size as well as area at risk (21,32). Isoflurane (1.5% inhaled via nose cone) was used during ischemia and avertin (0.005 ml/g) was used for sedation for imaging at 1 and 2 weeks based on previously established methods for infarct quantitation in vivo (31).

Histologic analysis

Two weeks after I/R injury in vivo, the mice were euthanized, and the mouse hearts were removed and weighed to determine the HW/BW ratio. Mouse hearts were processed, paraffin-embedded, and stained with H&E, Masson's trichrome, and Picrosirius red staining, as described (20). To estimate the volume fraction (%) of collagen, serial sections of Masson's trichrome– or Picrosirius red–stained sections were quantified using color thresholding by ImageJ software (NIH), and data were expressed as the average percentage of the LV stained. Two midpapillary sections per heart (n = 5–6 per group) were quantified. To evaluate myocyte size, sections were deparaffinized, rehydrated, and stained with fluorescent rhodamine–conjugated wheat germ agglutinin at 5μg/ml in 1% BSA, 1× TBS (Vector Laboratories). Fluorescence was visualized using a Zeiss confocal microscope, and digital images were analyzed and measured with Zeiss Axiovision software (34).

RNA extraction and microarray analysis

Hearts from 10- to 12-week-old male WT, *Myh6*-TRAF2$_{LC}$, *Myh6*-IκBαΔN, and *Myh6*-TRAF2$_{LC}$/*Myh6*-IκBαΔN (n = 4 per group) mice were used for transcriptional profiling. Total RNA was extracted from mouse hearts using the RNEasy Fibrous Tissue Midi kit (Qiagen), according to the manufacturer's instructions. Gene expression analysis was performed using the Sentrix BeadChip and BeadStation system from Illumina Inc. RNA was further processed and hybridized to a Mouse Ref-6 BeadChip array (Illumina Inc.). The mouse Ref-6 BeadChips contain sequences representing approximately 46,000 curated genes and ESTs. After scanning the probe array, the resulting image was analyzed using the BeadStudio software (Illumina Inc.). Samples were normalized using a cubic spline procedure, and the average signal for each probeset was determined. All such average probe set signals were used to determine intra- and intergroup variance using a principal components analysis plot in Partek Genome Studio 6.6 (Partek). Differentially expressed genes were assessed using 1-way ANOVA model with contrasts in Partek Genome Studio 6.6, with a cutoff of an absolute fold-change above 1.2 and FDR < 0.05, unless otherwise noted. Selected differentially expressed gene profiles across all 16 mouse hearts were displayed using unsupervised hierarchical clustering with Euclidean distance and average linkage (Partek Genome Studio 6.6). Microarray data has been deposited to the NCBI Gene Expression Omnibus (GEO GSE107668).

Activation of NF-κB and STAT3

We used 2 different approaches to assess NF-κB activation in the hearts of the WT, *Myh6*-TRAF2$_{LC}$, *Myh6*-IκBαΔN, and *Myh6*-TRAF2$_{LC}$/*Myh6*-IκBαΔN mice. Whole heart tissue from 10- to 12-week-old male mice was homogenized and separated into cytoplasmic and nuclear fractions using the NE-PER Nuclear and Cytoplasmic Extraction reagents (ThermoFisher Scientific). We first performed Western blotting for RelB (catalog 4954, Cell Signaling Technology), p50 (catalog 32360, Abcam), p52 (catalog 4882, Cell Signaling Technology), and p65 (catalog 8242, Cell Signaling Technology) in nuclear and cytosolic extracts. For loading controls, the samples for nuclear extracts were normalized by RNA pol II (catalog 05-623, MilliporeSigma), whereas GAPDH (catalog 22555, Abcam) was used as a loading control for cytosolic extracts. Western blotting was also performed for NIK on total cell lysates (catalog 4994, Cell Signaling Technology). Protein expression was visualized using horseradish peroxidase–conjugated donkey anti-rabbit or donkey anti-mouse secondary antibody (1:5,000; Cell Signaling Technology) and Pierce Supersignal West Dura Extended Duration Substrate (ThermoFisher Scientific) and detected using the Kodak Imagine Station 4000$_R$ Pro.

We also examined NF-κB activation in nuclear extracts from 10- to 12-week-old male WT, *Myh6*-TRAF2$_{LC}$, *Myh6*-IκBαΔN, and *Myh6*-TRAF2$_{LC}$/*Myh6*-IκBαΔN mouse hearts, using the TransAM NF-kB family transcription factor assay (Active Motif), according to manufacturer's instructions (17). Ninety-six–well plates coated with a DNA probe containing the NF-κB consensus binding site were incubated with 20 μg of nuclear extract, followed by incubation with antibodies to p65, p50, p52, or RelB included in the kit. HRP-conjugated secondary antibody incubation was then performed and the plate was developed. Absorbance was measured with the Bio-Rad 680 Microplate Reader. Data represent the average of duplicate samples from each heart.

To determine STAT3 activation in WT and *Myh6*-TRAF2$_{LC}$ mouse hearts, Western blotting was performed on nuclear and cytosolic myocardial extracts from 12-week-old mouse hearts that were subjected to the same ex vivo I/R protocol described above with the diluent or 10 μM AG490. Mouse hearts were collected after the first 15 minutes of reperfusion for lysate preparation. We measured phospho-STAT3 using an antibody (catalog 9145, Cell Signaling Technology) that measures Tyr705 phosphorylation, which is responsible for STAT3 activation, dimerization, nuclear translocation, and DNA binding (35). The blots

were stripped using the Restore Plus Western Blot Stripping Buffer (ThermoFisher Scientific) and reprobed with an antibody to total STAT3 (catalog 9139, Cell Signaling Technology), and the final results were expressed as the ratio of phosphorylated STAT3/total STAT3.

ChIP assay and qPCR

ChIP assay was performed on *Tnip1* and *Nfkbie*, which were chosen as candidate genes whose expression was mediated by NF-κB–mediated signaling. ChIP assay was performed using the EZ-ChIP Assay Kit (MilliporeSigma) following the manufacturer's instructions, exactly as described previously (13). Chromatin was immunoprecipitated with antibodies against NF-κB family members (RelB, sc-226, Santa Cruz Biotechnology Inc.; p50, ab7971, Abcam; p65, catalog 8242, Cell Signaling Technology; p52, ab7972, Abcam) or control antibodies overnight at 4°C with rotation. PCR was performed with 4 μl of immunoprecipitated DNA using the following primers for the *Tnip1* promoter: forward 5′ GACTCAGCAAGACTCAGCATC 3′, reverse 5′ TCAAGCAAAGGCAGGTACAA 3′. *Tnip1* primers were based on a consensus κB site predicted in the mouse promoter by PROMO (http://alggen.lsi.upc.es/cgi-bin/promo_v3/promo/promoinit.cgi?dirDB=TF_8.3) 383 bp upstream of the transcription start site. Gurevich et al. also described consensus κB sites in similar locations in the human *Tnip1* promoter (36).

The following primers were used for the *Nfkbie* promoter: forward 5′CACGCAGGAGTGAGTCAAGA 3′, reverse 5′ AAAGGAGCTTCCGGGTAGAG 3′ (37). *Tnip1* and *Nfkbie* mRNA expression were confirmed by qPCR and Western blotting in 12-week-old WT, *Myh6*-TRAF2$_{LC}$, *Myh6*-IκBαΔN, and *Myh6*-TRAF2$_{LC}$/*Myh6*-IκBαΔN mouse hearts. qPCR was performed on an ABI 7500 Fast Real-Time PCR System (Applied Biosystems). RNA (2 μg of total) was reverse-transcribed into cDNA using SuperScript III First strand synthesis system (ThermoFisher Scientific). cDNAs were then evaluated for 18S rRNA (catalog 4333760F), *Tnip1* (Mm01288484_m1), and *Nfkbie* (Mm01269649_m1) content using TaqMan gene expression assay (Applied Biosystems). Western blotting was performed using a monoclonal antibody for ABIN-1 (*Tnip1*) (catalog 37-6100, Invitrogen) and a polyclonal antibody for IκBε (catalog AF4637, R&D systems); GAPDH (catalog 22555, Abcam) was used as the loading control.

Statistics

Data are expressed as means ± SEM. One-way ANOVA with Bonferroni post-hoc analysis (Graphpad Prism) was used to test for differences in HW/BW ratios, CK release, EBD uptake, densitometry, Trichrome and Picrosirius red staining, cell area, and qPCR, whereas *t* tests (2-tailed) were used when comparing only 2 groups. For repeated measures analysis, (2-D echocardiograhic and Langendorff perfusion data), mixed models methodology was used. Group, time, and the interaction between group and time were all entered into the model. Time was treated as a categorical variable. The interaction was evaluated to determine if the relationship between group and LVDP varied with respect to time. Based on the Akaike Information Criteria (AIC) and Shwarz Information Critieria (BIC), an unstructured variance-covariance matrix was used to model the repeated measurements. Group means were based on model results, and differences between groups were determined overall and within each time point. All pair-wise comparisons were considered. Test results were adjusted based on Sidak's method to control the overall type I error rate. A value of $P < 0.05$ was considered statistically significant.

Study approval

All studies were performed with the approval of the IACUC at Washington University School of Medicine. These investigations conform to the *Guide for the Care and Use of Laboratory Animals* (National Academies Press, 2011).

Author contributions

SE performed experiments, analyzed data, performed statistical analysis, and assisted in manuscript preparation. HPT performed experiments and analyzed data. DVN provided technical advice and assisted with interpretation and experimental design. SM contributed to gene array experiments and assisted with reviewing and revising the manuscript. CW and AK assisted with in vivo mouse experiments and the review of the manuscript. PMB assisted with experimental design and the review of the manuscript. DLM conceived the studies, assisted with technical advice and experimental design, and wrote the manuscript draft. All authors reviewed and revised the manuscript.

Acknowledgments

This study was supported by research funds from NIH R01 HL 111094, R01 HL58081, and R01 HL089543. The authors would like to thank Lora Staloch for her technical support.

Address correspondence to: Douglas L. Mann, Division of Cardiology, 660 S. Euclid Avenue, Campus Box 8086, St. Louis, Missouri 63110, USA. Phone: 314.362.8908; Email: dmann@dom.wustl.edu.

1. Mann DL. Stress-activated cytokines and the heart: from adaptation to maladaptation. *Annu Rev Physiol*. 2003;65:81–101.
2. Gang H, Shaw J, Dhingra R, Davie JR, Kirshenbaum LA. Epigenetic regulation of canonical TNFα pathway by HDAC1 determines survival of cardiac myocytes. *Am J Physiol Heart Circ Physiol*. 2013;304(12):H1662–H1669.
3. Nakano M, Knowlton AA, Dibbs Z, Mann DL. Tumor necrosis factor-alpha confers resistance to hypoxic injury in the adult mammalian cardiac myocyte. *Circulation*. 1998;97(14):1392–1400.
4. Eddy LJ, Goeddel DV, Wong GH. Tumor necrosis factor-alpha pretreatment is protective in a rat model of myocardial ischemia-reperfusion injury. *Biochem Biophys Res Commun*. 1992;184(2):1056–1059.
5. Kurrelmeyer KM, et al. Endogenous tumor necrosis factor protects the adult cardiac myocyte against ischemic-induced apoptosis in a murine model of acute myocardial infarction. *Proc Natl Acad Sci USA*. 2000;97(10):5456–5461.
6. Lecour S, Smith RM, Woodward B, Opie LH, Rochette L, Sack MN. Identification of a novel role for sphingolipid signaling in TNF alpha and ischemic preconditioning mediated cardioprotection. *J Mol Cell Cardiol*. 2002;34(5):509–518.
7. Deuchar GA, Opie LH, Lecour S. TNFalpha is required to confer protection in an in vivo model of classical ischaemic preconditioning. *Life Sci*. 2007;80(18):1686–1691.
8. Lecour S. Activation of the protective Survivor Activating Factor Enhancement (SAFE) pathway against reperfusion injury: Does it go beyond the RISK pathway? *J Mol Cell Cardiol*. 2009;47(1):32–40.
9. Burchfield JS, et al. The cytoprotective effects of tumor necrosis factor are conveyed through tumor necrosis factor receptor-associated factor 2 in the heart. *Circ Heart Fail*. 2010;3(1):157–164.
10. Guo X, et al. Cardioprotective Role of Tumor Necrosis Factor Receptor-Associated Factor 2 by Suppressing Apoptosis and Necroptosis. *Circulation*. 2017;136(8):729–742.
11. Yang KC, et al. Tumor necrosis factor receptor-associated factor 2 mediates mitochondrial autophagy. *Circ Heart Fail*. 2015;8(1):175–187.
12. Xie P. TRAF molecules in cell signaling and in human diseases. *J Mol Signal*. 2013;8(1):7.
13. Tzeng HP, et al. Dysferlin mediates the cytoprotective effects of TRAF2 following myocardial ischemia reperfusion injury. *J Am Heart Assoc*. 2014;3(1):e000662.
14. Papathanasiou S, et al. Tumor necrosis factor-α confers cardioprotection through ectopic expression of keratins K8 and K18. *Nat Med*. 2015;21(9):1076–1084.
15. Lecour S, et al. Pharmacological preconditioning with tumor necrosis factor-alpha activates signal transducer and activator of transcription-3 at reperfusion without involving classic prosurvival kinases (Akt and extracellular signal-regulated kinase). *Circulation*. 2005;112(25):3911–3918.
16. Lacerda L, Somers S, Opie LH, Lecour S. Ischaemic postconditioning protects against reperfusion injury via the SAFE pathway. *Cardiovasc Res*. 2009;84(2):201–208.
17. Divakaran VG, et al. Tumor necrosis factor receptor-associated factor 2 signaling provokes adverse cardiac remodeling in the adult mammalian heart. *Circ Heart Fail*. 2013;6(3):535–543.
18. Cildir G, Low KC, Tergaonkar V. Noncanonical NF-κB Signaling in Health and Disease. *Trends Mol Med*. 2016;22(5):414–429.
19. Sun SC. The noncanonical NF-κB pathway. *Immunol Rev*. 2012;246(1):125–140.
20. Lavine KJ, et al. Coronary collaterals predict improved survival and allograft function in patients with coronary allograft vasculopathy. *Circ Heart Fail*. 2013;6(4):773–784.
21. Zhang Y, et al. Validation of the wall motion score and myocardial performance indexes as novel techniques to assess cardiac function in mice after myocardial infarction. *Am J Physiol Heart Circ Physiol*. 2007;292(2):H1187–H1192.
22. Verstrepen L, Carpentier I, Verhelst K, Beyaert R. ABINs: A20 binding inhibitors of NF-kappa B and apoptosis signaling. *Biochem Pharmacol*. 2009;78(2):105–114.
23. Misra A, et al. Nuclear factor-kappaB protects the adult cardiac myocyte against ischemia-induced apoptosis in a murine model of acute myocardial infarction. *Circulation*. 2003;108(25):3075–3078.
24. Basak S, et al. A fourth IkappaB protein within the NF-kappaB signaling module. *Cell*. 2007;128(2):369–381.
25. Gordon JW, Shaw JA, Kirshenbaum LA. Multiple facets of NF-κB in the heart: to be or not to NF-κB. *Circ Res*. 2011;108(9):1122–1132.
26. Sun SC. Non-canonical NF-κB signaling pathway. *Cell Res*. 2011;21(1):71–85.
27. Shen RR, et al. TRAF2 is an NF-κB-activating oncogene in epithelial cancers. *Oncogene*. 2015;34(2):209–216.
28. Lo D, Quill H, Burkly L, Scott B, Palmiter RD, Brinster RL. A recessive defect in lymphocyte or granulocyte function caused by an integrated transgene. *Am J Pathol*. 1992;141(5):1237–1246.
29. Birnbaum Y, Hale SL, Kloner RA. Differences in reperfusion length following 30 minutes of ischemia in the rabbit influence infarct size, as measured by triphenyltetrazolium chloride staining. *J Mol Cell Cardiol*. 1997;29(2):657–666.
30. Nossuli TO, et al. A chronic mouse model of myocardial ischemia-reperfusion: essential in cytokine studies. *Am J Physiol Heart Circ Physiol*. 2000;278(4):H1049–H1055.
31. Lavine KJ, Kovacs A, Weinheimer C, Mann DL. Repetitive myocardial ischemia promotes coronary growth in the adult mammalian heart. *J Am Heart Assoc*. 2013;2(5):e000343.
32. Kanno S, et al. Echocardiographic evaluation of ventricular remodeling in a mouse model of myocardial infarction. *J Am Soc*

Echocardiogr. 2002;15(6):601–609.
33. Weinheimer CJ, Lai L, Kelly DP, Kovacs A. Novel mouse model of left ventricular pressure overload and infarction causing predictable ventricular remodelling and progression to heart failure. *Clin Exp Pharmacol Physiol*. 2015;42(1):33–40.
34. Lavine KJ, et al. Distinct macrophage lineages contribute to disparate patterns of cardiac recovery and remodeling in the neonatal and adult heart. *Proc Natl Acad Sci USA*. 2014;111(45):16029–16034.
35. Darnell JE, Kerr IM, Stark GR. Jak-STAT pathways and transcriptional activation in response to IFNs and other extracellular signaling proteins. *Science*. 1994;264(5164):1415–1421.
36. Gurevich I, Zhang C, Encarnacao PC, Struzynski CP, Livings SE, Aneskievich BJ. PPARγ and NF-κB regulate the gene promoter activity of their shared repressor, TNIP1. *Biochim Biophys Acta*. 2012;1819(1):1–15.
37. Hochrainer K, Racchumi G, Anrather J. Site-specific phosphorylation of the p65 protein subunit mediates selective gene expression by differential NF-κB and RNA polymerase II promoter recruitment. *J Biol Chem*. 2013;288(1):285–293.